

Structure and equation of state of Ti-bearing davemaoite: New insights into the chemical heterogeneity in the lower mantle

KENG-HSIEN CHAO^{1,2,‡}, MERYEM BERRADA², SIHENG WANG², JULIANA PECKENPAUGH^{1,2},
DONGZHOU ZHANG^{2,3}, STELLA CHARITON³, VITALI PRAKAPENKA³, AND BIN CHEN^{2,*;†}

¹Department of Earth Sciences, University of Hawaii at Manoa, Honolulu, Hawaii 96822, U.S.A.

²Hawaii Institute of Geophysics and Planetology, University of Hawaii at Manoa, Honolulu, Hawaii 96822, U.S.A.

³Center for Advanced Radiation Sources, The University of Chicago, 5640 S. Ellis, Chicago, Illinois 60637, U.S.A.

ABSTRACT

Davemaoite (CaSiO₃ perovskite) is considered the third most abundant phase in the pyrolytic lower mantle and the second most abundant phase in the subducted mid-ocean ridge basalt (MORB). During the partial melting of the pyrolytic upper mantle, incompatible titanium (Ti) becomes enriched in the basaltic magma, forming Ti-rich MORB. Davemaoite is considered an important Ti-bearing mineral in subducted slabs by forming a Ca(Si,Ti)O₃ solid solution. However, the crystal structure and compressibility of Ca(Si,Ti)O₃ perovskite solid solution at relevant pressure and temperature conditions had not been systematically investigated. In this study, we investigated the structure and equations of state of Ca(Si_{0.83}Ti_{0.17})O₃ and Ca(Si_{0.75}Ti_{0.25})O₃ perovskites at room temperature up to 82 and 64 GPa, respectively, by synchrotron X-ray diffraction (XRD). We found that both Ca(Si_{0.83}Ti_{0.17})O₃ and Ca(Si_{0.75}Ti_{0.25})O₃ perovskites have a tetragonal structure up to the maximum pressures investigated. Based on the observed data and compared to pure CaSiO₃ davemaoite, both Ca(Si_{0.83}Ti_{0.17})O₃ and Ca(Si_{0.75}Ti_{0.25})O₃ perovskites are expected to be less dense up to the core-mantle boundary (CMB), and specifically ~1–2% less dense than CaSiO₃ davemaoite in the pressure range of the transition zone (15–25 GPa). Our results suggest that the presence of Ti-bearing davemaoite phases may result in a reduction in the average density of the subducting slabs, which in turn promotes their stagnation in the lower mantle. The presence of low-density Ti-bearing davemaoite phases and subduction of MORB in the lower mantle may also explain the seismic heterogeneity in the lower mantle, such as large low shear velocity provinces (LLSVPs).

Keywords: Ti-bearing davemaoite, perovskite, Ca(Si,Ti)O₃ solid solution, equation of state, slab stagnation, density; Physics and Chemistry of Earth's Deep Mantle and Core

INTRODUCTION

Seismic observations and mineral physics studies have provided a comprehensive understanding of the mineralogy of the Earth's mantle (Dziewonski and Anderson 1981; Kaminsky 2012). According to the pyrolytic composition model for the mantle, davemaoite, a perovskite-structured CaSiO₃, is widely considered the third most abundant phase in the lower mantle (Kesson et al. 1998; Murakami et al. 2005; Ringwood 1962; Sun et al. 2016), making up an estimated 6–12% of its volume. This is supported by the discovery of davemaoite as inclusion in superdeep diamonds (Anzolini et al. 2018, 2016; Tschauner et al. 2021). Furthermore, davemaoite is the second most abundant phase in subducted oceanic crust, comprising an estimated 23–30% due to the higher Ca content of oceanic crust and surpassed only by bridgmanite (Hirose et al. 2005; Kesson et al. 1994; Kudo et al. 2012; Steeve et al. 2019; Stixrude and Lithgow-Bertelloni 2012). Nestola et al. (2018) found evidence

of inclusions of davemaoite in diamond originating from the subducted oceanic crust. The seismic velocity of the subducted oceanic crust or davemaoite can be used to explain the presence of the large low shear velocity provinces (LLSVPs), as suggested by Thomson et al. (2019).

Numerous studies have been conducted over the past several decades to investigate the physical and chemical properties of davemaoite, given its abundance and importance. Previous studies have focused on the structure and equations of state of davemaoite (Mao et al. 1989; Yagi et al. 1989; Shim et al. 2000a, 2000b, 2002; Kawai and Tsuchiya 2014; Chen et al. 2018; Sun et al. 2022); sound velocities or elastic properties at high pressures (Tamai and Yagi 1989; Akber-Knutson et al. 2002; Steeve et al. 2019; Thomson et al. 2019); the synthesis of davemaoite (Liu and Ringwood 1975); its phase transition at high pressure-temperature (*P-T*) conditions (Komabayashi et al. 2007); and its presence as diamond inclusions (Nestola et al. 2018; Tschauner et al. 2021). However, there is still little consensus on the structure and physical properties of davemaoite, particularly its equation of state (EoS) and elastic properties, primarily due to the fact that davemaoite is unquenchable and readily converts to glass after decompression

* Corresponding author E-mail: binchen@hawaii.edu

† Special collection papers can be found online at our website in the Special Collection section.

‡ Orcid <https://orcid.org/0000-0002-0329-7511>

(Liu and Ringwood 1975; Mao et al. 1989). This unrecoverable nature prevents the synthesized davemaoite from being further analyzed at ambient conditions.

Furthermore, davemaoite formed within the subducted slabs may contain considerable amounts of Ti by forming $\text{Ca}(\text{Si,Ti})\text{O}_3$ solid solution, as Ti is an incompatible element that tends to enrich in basaltic magma during partial melting of the upper mantle (Corgne and Wood 2005; Hirose et al. 2004), which then in turn forms the Ti-rich mid-ocean ridge basalt (MORB) (Gale et al. 2013; Hirose et al. 2005, 2004; Ricolleau et al. 2010). When the oceanic plates subduct to the lower mantle, Ti-rich davemaoite phase may form from the MORB under high-pressure and high-temperature conditions of the mantle. Indeed, $\text{Ca}(\text{Si,Ti})\text{O}_3$ perovskite as inclusions in superdeep diamonds were found to contain high Ti, as much as ~40–60 mol% of CaTiO_3 in the solid solution (Thomson et al. 2016).

If mantle heterogeneity such as LLSVPs is the result of the enrichment of recycled oceanic material as proposed by Thomson et al. (2019), the physical properties of Ti-bearing davemaoite should also be investigated to provide better reference to real geological conditions. The basic understanding of the series of Ti-rich $\text{Ca}(\text{Si,Ti})\text{O}_3$ perovskites was previously experimentally investigated by Leinenweber et al. (1997) and Sinelnikov et al. (1998). However, Leinenweber et al. (1997) focused on investigating the structure and lattice parameters of $\text{Ca}(\text{Ti}_x\text{Si}_{1-x})\text{O}_3$ at ambient conditions, where $1 > x > 0.65$, after quenching from multi-anvil press synthesis; Sinelnikov et al. (1998) focused on reporting the data of $\text{Ca}(\text{Si}_{0.23}\text{Ti}_{0.77})\text{O}_3$ and $\text{Ca}(\text{Si}_{0.49}\text{Ti}_{0.51})\text{O}_3$ for the composition between CaSiO_3 and CaTiO_3 . The maximum pressure reached by Sinelnikov et al. (1998) was also limited to 15 GPa. According to Leinenweber et al. (1997) and Sinelnikov et al. (1998), the introduction of Ti into the solid-solution system substantially changes the structure, unit-cell volume, and elastic properties of the solid solution under ambient conditions. Thus, it is likely that Ti in the subducted MORB also changes elastic properties and structure of davemaoite, likely contributing to the chemical and seismic heterogeneity in the deep mantle. Diamond-hosted $\text{Ca}(\text{Si,Ti})\text{O}_3$ inclusions were found to contain a wide range of Ti, with Ti content equivalent to 0–10 mol% CaTiO_3 to as high as ~40–60 mol% (Thomson et al. 2016). Therefore, it is crucial to investigate the effect of Ti on the structure and elastic properties of $\text{Ca}(\text{Si,Ti})\text{O}_3$ under the relevant pressure conditions of the lower mantle.

To gain a better understanding of the density and compressibility of Ti-rich davemaoite under relevant mantle conditions, we investigated the structure, density and bulk modulus of $\text{Ca}(\text{Si}_{0.83}\text{Ti}_{0.17})\text{O}_3$ and $\text{Ca}(\text{Si}_{0.75}\text{Ti}_{0.25})\text{O}_3$ davemaoite, referred to as 17TiPv and 25TiPv thereafter, up to ~82 and ~64 GPa, respectively. Our study reveals that the incorporation of Ti into CaSiO_3 to form $\text{Ca}(\text{Si,Ti})\text{O}_3$ solid solution results in a significant decrease in its density. This finding has implications for understanding mantle dynamics, as a subducting slab enriched in Ti can become stagnant at the transition zone (Fukao et al. 2001, 2009) due to the enrichment of the lower density of the Ti-bearing davemaoite. The enrichment of Ti-bearing davemaoite also can likely lead to the seismologically observed low-density feature in the lower mantle, such as LLSVPs (Hernlund and Houser 2008; Deschamps et al. 2012, 2012; Frost and Rost 2014).

EXPERIMENTAL METHODS

We prepared $\text{Ca}_{1.08}\text{Si}_{0.83}\text{Ti}_{0.17}\text{O}_{3.08}$ and $\text{Ca}_{1.02}\text{Si}_{0.75}\text{Ti}_{0.25}\text{O}_{3.02}$ glass as our starting materials. Both starting materials were prepared by mixing and grinding appropriate stoichiometric ratios (100:17:83 and 4:3:1 in the molar fraction, respectively) CaCO_3 , TiO_2 , and SiO_2 together with acetone in the agate mortar. For each composition, the mixture was placed in a platinum crucible in an oven at 200 °C overnight to remove moisture. The dehydrated mixture was then heated to 900 °C overnight to decarbonate the CaCO_3 portion into CaO, followed by heating to 1600 °C until fully molten. The molten glass was then rapidly quenched with a water bath.

The quenched 17TiPv and 25TiPv glass was recovered from the crucible and broken into fragments of ~1–2 mm in size and cast into epoxy. Chemical compositions were determined using the electron probe microanalysis (EPMA) method using the field emission electron microprobe JEOL JXA-8500F in the Department of Earth Sciences of the University of Hawaii, with an acceleration voltage of 15–20 keV, a current of 20–30 A, and a spot size of up to 5 μm . Pure CaTiSiO_3 sphene was used as the standard to calibrate Ca, Si, and Ti. The average chemical compositions of 17TiPv glass and 25TiPv glass are $\text{Ca}_{1.08}\text{Si}_{0.83}\text{Ti}_{0.17}\text{O}_{3.08}$ and $\text{Ca}_{1.02}\text{Si}_{0.75}\text{Ti}_{0.25}\text{O}_{3.02}$, respectively (Online Materials¹ Tables S1 and S2). The chemical composition was homogeneous between the probe points in both samples. Based on such chemical compositions, the (Si+Ti):O should be 1:3 in chemical formula of perovskite structure, and there may be a trace amount of excess CaO (<4 wt%). The phases after laser heating would be $\text{Ca}(\text{Si,Ti})\text{O}_3$ with minor CaO, although the CaO was not detected by high pressure X-ray diffraction (XRD) experiments of $\text{Ca}(\text{Si,Ti})\text{O}_3$ perovskites in the later part of this study.

The 17TiPv and 25TiPv glass recovered from the crucible were further ground into finer grains within 10–100 μm . A few grains of each sample were loaded into diamond-anvil cells (DAC) with neon using the gas-loading system at GSECARS, Advanced Photon Source, Argonne National Laboratory (Rivers et al. 2008). A short symmetric DAC with diamonds of 250 μm in culet size was used for 17TiPv glass and a regular symmetric DAC with diamonds of 300 μm in culet size was used for 25TiPv, respectively. X-ray diffraction experiments were performed at Beamline 13-IDD of the Advanced Photon Source, Argonne National Laboratory. The wavelength of the X-ray was 0.2952 Å. In the experimental setup, the Pilatus 1 M CdTe detector calibrated by the powder LaB_6 NIST standard was used at a distance of 207 mm from the diamond-anvil cell. 17TiPv glass and 25TiPv glass were compressed to ~20 and ~15 GPa, respectively. The sample was then heated by a double-sided laser heating system using the 100 W fiber laser (IPG Photonics) with a wavelength of 1064 nm and a spot size of 12 μm flat top. After being heated to high temperatures above 1800 K, the glass sample turned into an opaque perovskite phase. When the formation of the perovskite phase was detected by X-ray diffraction (XRD), the laser heating was repeated several times to completely transform the glass into crystalline phases. We collected XRD data on the synthesized perovskite samples that were compressed to ~82 and ~64 GPa for 17TiPv and 25TiPv, respectively, with a typical pressure interval of 2–3 GPa by the gas membrane at 300 K. At each pressure point, a step scan XRD measurement was performed for 17TiPv and 25TiPv, with a step interval of 0.5°, total rotation range of 34° and 25°. The collection time was one second per step and 2 s per step for 17TiPv and 25TiPv, respectively.

XRD images with masked diamond peaks were integrated into 1D diffraction patterns using Dioptas software (Prescher and Prakapenka 2015). Unit-cell volumes of gold were determined by PDIndexer (Seto et al. 2010), which were subsequently used to determine the sample pressures using the EoS by Fei et al. (2007). PeakPo (Shim 2020) and GSAS-II were used to analyze the lattice parameters of the diffraction pattern of Ti-bearing davemaoite (Online Materials¹ Fig. S1). After determining the lattice parameters, unit-cell volume, as well as pressure points, we used EoSFit7-GUI (Gonzalez-Platas et al. 2016) and Pythoes (Shim 2017) to calculate the second-order Birch-Murnaghan EoS of 17TiPv and 25TiPv.

RESULTS AND DISCUSSION

Syntheses and structures of $\text{Ca}(\text{Si,Ti})\text{O}_3$ perovskites

The amorphous samples were compressed to a pressure of ~15–20 GPa, within the stability field of the Ca-perovskite phase (Milani et al. 2021). Afterward, we conducted a wide-scan XRD measurements before and after heating to identify the formation of the perovskite phase. As expected, the XRD pattern of the samples before heating showed amorphous scattering. However, the perovskite peaks appeared upon laser heating to ~2000 K,

as shown in Figure 1.

The synthesized 17TiPv and 25TiPv perovskites both exhibited a tetragonal structure. The subtle splitting of the peaks of the tetragonal perovskite phase, (200), (002), (211), (112), is apparent in 17TiPv (Fig. 1a). In contrast, such splitting is more subtle in 25TiPv: only showing a shoulder or overlap each other, but still distinguishable (Fig. 1b). The pressure of 17TiPv became 27.2 GPa after laser heating at ~20 GPa. The pressure of 25TiPv did not change significantly, slightly changing from 15 to 15.5 GPa after laser heating.

Representative XRD patterns of 17TiPv and 25TiPv are shown in Figure 2 with a focus on the 2θ range of 6–15°, where most of the peaks are strong and distinguishable. The representative full range XRD raw data are shown in Online Materials¹ Figure S2. The peaks with corresponding d -spacing are normalized to the maximum intensity of the first two overlapping diffraction peaks of the perovskite structure, (112) + (200) and (110) + (101) for 17TiPv and 25TiPv, respectively. Our observations agree well with the space group of $I4/mcm$ and $P4/mmm$ for 17TiPv

and 25TiPv, respectively. Several possible space groups have been reported for pure CaSiO_3 , $I4/mmm$, $P4/mmm$, $P4/mbm$, and $I4/mcm$ (Shim et al. 2002), all of which could be observed given that there is subtle difference in free energy among them and the experimental XRD pattern would be sensitive to local stress and pressure gradient in the DAC (Chen et al. 2018). According to Chen et al. (2018), the expected XRD pattern of $I4/mcm$ has an XRD pattern similar to that of $P4/mmm$, but with an additional peak (211), between the equivalent positions of (110) and (111) of the ideal cubic perovskite structure. Our XRD data show that the peak (211) is present in 17TiPv but not in 25TiPv. Other space groups, $I4/mmm$ and $P4/mbm$ reported by Shim et al. (2002) also contain additional peaks between the equivalent positions of (110) and (111) of the ideal cubic perovskite structure with a 2θ lower than that of (211) of $I4/mcm$. These peaks are not observed in both 17TiPv and 25TiPv, suggesting $I4/mcm$ and $P4/mmm$ structures for 17TiPv and 25TiPv, respectively. The observed 2θ and the corresponding d -spacing of the representative XRD pattern of 17TiPv and 25TiPv agree well with the calculated

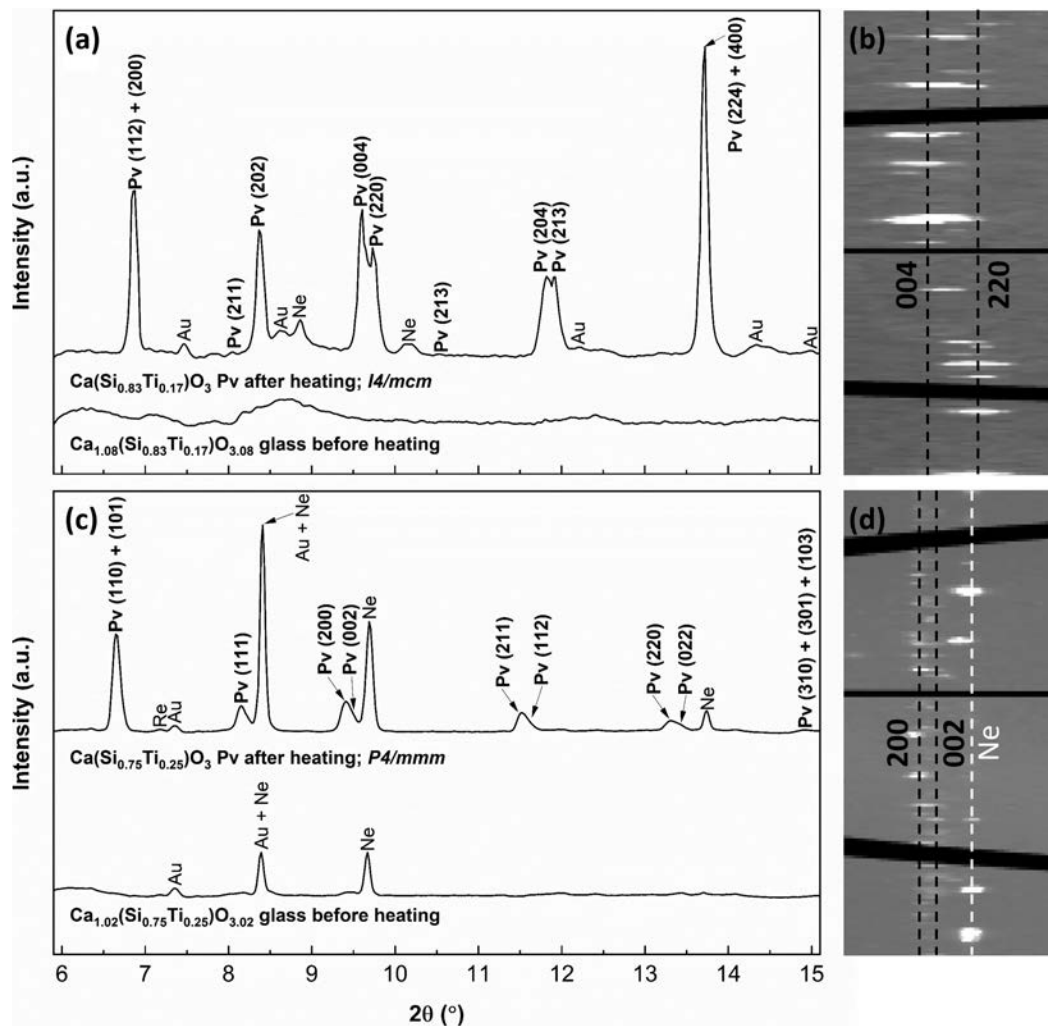
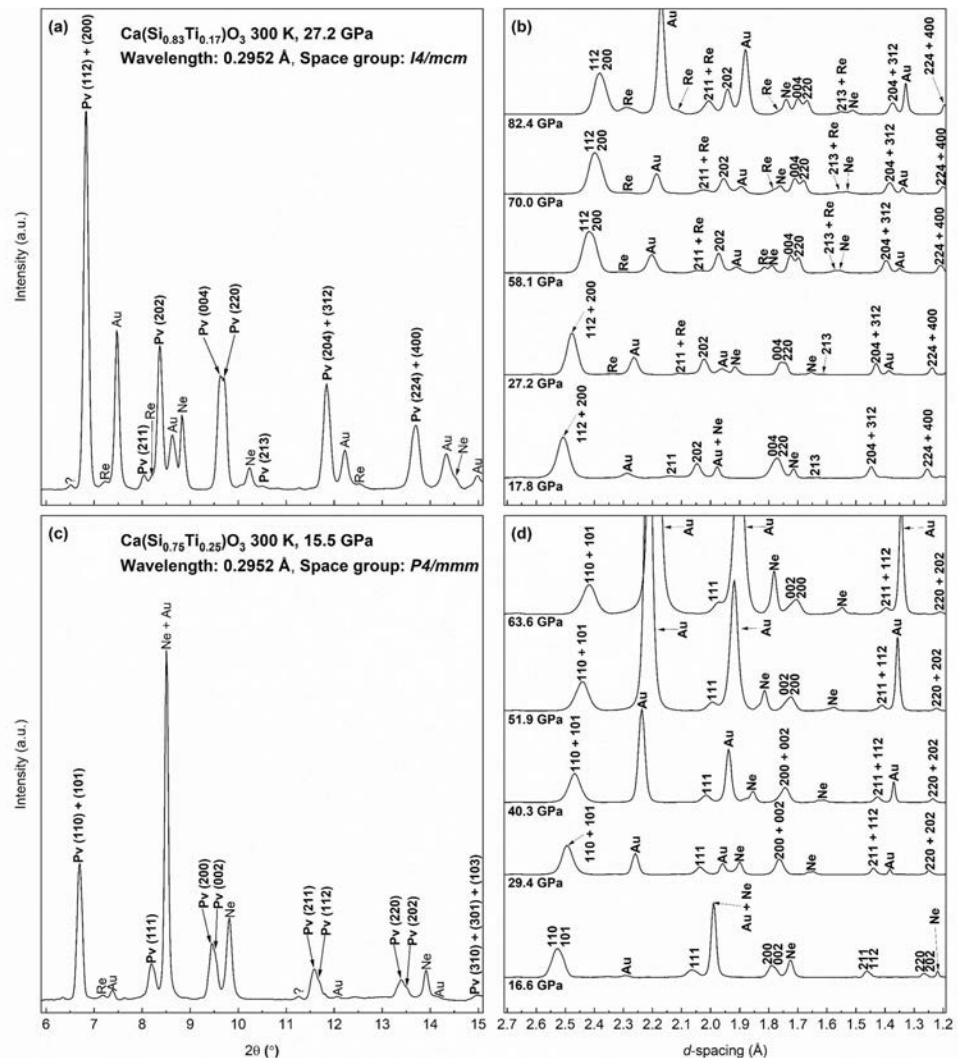


FIGURE 1. (a) Integrated XRD patterns before and after heating of 17TiPv and (b) unrolled projections of the 2D raw diffraction areas near splitting (004) and (220) peaks of 17TiPv. (c) Integrated XRD patterns before and after heating of 25TiPv and (d) unrolled projections of the 2D raw diffraction areas near splitting (200) and (002) peaks of 25TiPv.

FIGURE 2. Representative integrated XRD patterns (a) and d -spacing (b) of 17TiPv, respectively. Representative integrated XRD patterns (c) and d -spacing (d) of 25TiPv, respectively. 17TiPv and 25TiPv are in $I4/mcm$ and $P4/mmm$ space group, respectively, based on our observation: 17TiPv ($I4/mcm$) has an additional peak (211) at around $2\theta = 8^\circ$, where such peak is not observed in 25TiPv ($P4/mmm$). Question marks are unidentified peaks.



values for their specific structures, which can be found in Online Materials¹ Tables S3 and S4.

The c/a ratios of 17TiPv and 25TiPv are compared with those of CaSiO_3 reported by Ono et al. (2004) and Sun et al. (2022) in Figure 3. Our study shows that the c/a ratios of both 17TiPv and 25TiPv increase monotonically with pressure. Ono et al. (2004) and Sun et al. (2022) show opposite pressure dependence of c/a ratio despite both studies report CaSiO_3 adopts $P4/mmm$ structure. The c/a ratio of CaSiO_3 , reported by Ono et al. (2004) and Sun et al. (2022) decreases and increases monotonically with rising pressure, respectively. Due to the sensitivity of structure of perovskites to the strain-stress condition (Chen et al. 2018), there is little consensus regarding the trend of pressure dependence of c/a ratio of davemaoite.

The structure of 17TiPv is demonstrated by analyzing the step-scan XRD pattern at 27.2 GPa (Fig. 2a). The XRD pattern shows that the (004) and (220) peaks split and can be recognized, indicating that 17TiPv adopts a tetragonal structure. We also observed the (211) peak at $2\theta \sim 8^\circ$, which is evidence of an $I4/mcm$ structure. The representative XRD pattern of 17TiPv with 2θ converted to d -spacing is shown in Figure 2b. We found

that the splitting of (004) and (220) becomes more obvious as the pressure increases. The c/a ratio of 17TiPv increases monotonically with pressure: c/a ratio = ~ 1.42 at ~ 7 GPa and rises to ~ 1.44 at ~ 82 GPa (Fig. 3). No pressure-induced phase transition is observed for 17TiPv up to 82 GPa.

The XRD data of 25TiPv were collected after the perovskite sample was synthesized at 15.5 GPa. We observed that at 15.5 GPa, most of the peaks have distinguishable shoulders [see peaks (200), (002), (211), (112), (220), and (202) in Fig. 2c]. However, we did not observe the peak (211) at $2\theta \sim 8^\circ$ for the structure $I4/mcm$, indicating that 25TiPv likely adopts a space group $P4/mmm$. Interestingly, we found that the c/a ratio becomes higher than 1.0 above ~ 32 GPa. In Figure 2d, at 16.6 GPa, (200) has a stronger intensity than (002), and (002) is presented as a shoulder with a lower d -spacing. At ~ 29 and ~ 40 GPa, the (200) and (002) almost overlapped each other, forming a symmetric (200) + (002) peak. As the pressure increases, the (200) + (002) peak becomes asymmetric again, and a shoulder appears at higher d -spacing. Chen et al. (2018) summarized the calculated relative positions and intensities of (200) and (002) in the $P4/mmm$ space group. The calculated (200) has a stronger

intensity than (002). If the c -axis has a shorter length than the a -axis, (200) has a lower 2θ (or higher d -spacing) than (002), and vice versa. Assuming that the relative intensity of diffraction peaks of 25TiPv generally follows the calculation, at 16.6 GPa, (200) has a stronger intensity and higher d -spacing than (002). This feature can be described by the crystal structure, $P4/mmm$ with $c < a$. Whereas, at ~ 52 and ~ 64 GPa, (200) has a stronger intensity and a lower d -spacing than (002), better described by the crystal structure, $P4/mmm$ with $c > a$. Interestingly, further data processing to constrain the lengths of a -axis and c -axis assuming that the relative intensities of (200) and (002) follow the theoretical calculation reveals that the c/a ratio becomes nearly one at ~ 32 GPa (Fig. 3). The c/a ratio of 25TiPv is ~ 0.99 at 15 GPa and temporarily becomes pseudocubic structure at 32 GPa when the c/a ratio approaches ~ 1.0 . However, the c/a ratio of 25TiPv continues to increase above 32 GPa without changing its structure $P4/mmm$, to ~ 1.015 at 64 GPa. Further investigations are needed to determine whether this feature is a potential phase transition by using the diamond-anvil cell with wider opening angle, which provides complete access to higher diffraction angle peaks for a comprehensive refinement of the structure.

Equation of state (EoS) of $a(\text{Si,Ti})\text{O}_3$ perovskites

The lattice parameters for 17TiPv and 25TiPv were determined from the XRD measurements (Online Materials¹ Tables S5 and S6). Unit-cell volumes under ambient conditions are not available, because the 17TiPv sample is not quenchable and became amorphous after being decompressed to ambient pressure, similar to pure CaSiO_3 davemaoite. The 25TiPv sample was compressed to 64 GPa, but the diamond broke under further compression. The observed value of unit-cell volumes, as well as fitted second-order Birch-Murnaghan EoS of 17TiPv and 25TiPv,

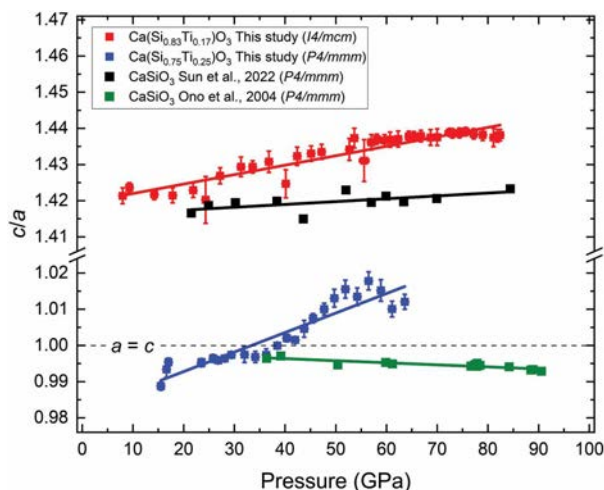


FIGURE 3. The c/a ratio of 17TiPv (red) and 25TiPv (blue) in this study, and CaSiO_3 reported by Ono et al. (2004) and Sun et al. (2022). Both 17TiPv and 25TiPv have c/a ratio increases monotonically with pressure. The 25TiPv has a c/a ratio becoming near 1.0 at 32 GPa without changing space group after 32 GPa. However, Ono et al. (2004) and Sun et al. (2022) reported opposite result regarding the c/a ratio of CaSiO_3 with the same space group observed. Therefore, the c/a ratio is sensitive to the stress strain condition of each study. (Color online.)

are shown in Figure 4. The formula units in the unit cell (Z) of $I4/mcm$ and $P4/mmm$ are $Z = 4$ and $Z = 1$, respectively. Molar volumes under ambient conditions (V_0) of 17TiPv and 25TiPv are 28.75 and 29.68 cm^3/mol , respectively. The calculated initial bulk moduli (K_0) of 17TiPv and 25TiPv are 224 ± 2 GPa and 205 ± 4 GPa, respectively, and their pressures derivatives of the bulk modulus (K') are all fixed at 4.0. The residuals are typically within $\pm 0.5\%$ (Online Materials¹ Fig. S3). Including or excluding decompression data has a minor effect on the second-order Birch-Murnaghan EoS of 17TiPv (Online Materials¹ Fig. S4). The stress-normalized pressure (f - F) figure (Online Materials¹ Fig. S4) shows both 17TiPv and 25TiPv have well-fit horizontal slopes in the f - F plot, suggesting their derivatives of the bulk modulus are near 4.0.

The EoS's of 17TiPv and 25TiPv were compared with those of pure CaSiO_3 davemaoite (Mao et al. 1989; Yagi et al. 1989; Shim et al. 2000a; Sun et al. 2022), and pure CaTiO_3 perovskite (Guennou et al. 2010) (Fig. 4), with the unit-cell volumes of all phases converted to molar volume. Despite the lack of consensus on the EoS of pure CaSiO_3 davemaoite, the molar volumes of all Ti-bearing phases investigated exceed those of pure CaSiO_3 davemaoite, with that of pure CaTiO_3 perovskite being the highest followed by 25TiPv and 17TiPv. Our results show that the molar volume of $\text{Ca}(\text{Si,Ti})\text{O}_3$ solid solutions increases monotonically with increasing Ti content, consistent with the relatively larger radius of Ti than that of Si. The EoS's of $\text{Ca}(\text{Si,Ti})\text{O}_3$ perovskites were summarized and their molar V_0 and K_0 were plotted as a function of Ti concentration (Table 1; Fig. 5) (Caracas et al. 2005; Chizmeshya et al. 1996; Fischer et al. 1993; Guennou et al. 2010; Jung and Oganov 2005; Kawai and Tsuchiya 2014; Kung and Rigden 1999; Leinenweber et al. 1997; Mao et al. 1989; Ono et al. 2004; Shim et al. 2000b, 2000a; Sinelnikov et al. 1998; Sun et al. 2022, 2016; Tarrida and Richet 1989; Thomson et al. 2019; Truffet et al. 2023; Wang et al. 1996; Yagi et al. 1989). Although the EoS of pure CaSiO_3 davemaoite remains controversial, there are two interesting features in Figure 5. First, in Figure 5a, the molar V_0 rises almost linearly with increasing Ti content. Leinenweber et al. (1997) showed that the $\text{Ca}(\text{Si,Ti})\text{O}_3$ solid solution has orthorhombic structure when molar fraction of CaTiO_3 is $>50\%$, and its tetragonal structure when the composition is exactly $\text{Ca}(\text{Si}_{0.5}\text{Ti}_{0.5})\text{O}_3$ or less Ti concentration. It is intriguing that the molar V_0 rises linearly with the Ti content, even if the whole solid solution undergoes a drastic change in symmetry. The molar V_0 of pure CaSiO_3 davemaoite is around 27.5 cm^3 , and the molar V_0 of pure CaTiO_3 perovskite is around 34 cm^3 . The compositions between CaSiO_3 and CaTiO_3 have a molar V_0 close to the trend line.

The K_0 is expected to decrease monotonically with Ti content, since Ti has a larger radius and is more compressible than Si. The dashed lines are plotted to guide the eyeline based on what we observed and current reported K_0 of the $\text{Ca}(\text{Si,Ti})\text{O}_3$ solid solution. The K_0 drops most dramatically from 17TiPv (~ 224 GPa) to 25TiPv (~ 209 GPa); then drops less drastically from 25TiPv to CaTiO_3 50% (~ 185 GPa). However, above CaTiO_3 50%, K_0 only barely drops across this compositional range, from 185 GPa at $\text{Ca}(\text{Si}_{0.5}\text{Ti}_{0.5})\text{O}_3$ to around 180 GPa in pure CaTiO_3 with a 50% increase in the molar fraction of CaTiO_3 . This could be because the $\text{Ca}(\text{Si,Ti})\text{O}_3$ solid solution

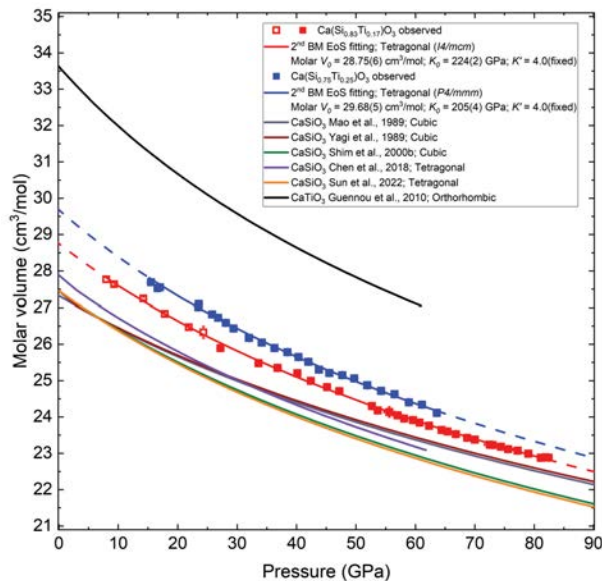


FIGURE 4. The comparison of Birch-Murnaghan equations of state among 17TiPv (red), 25TiPv (blue), pure CaSiO₃ (Chen et al. 2018; Mao et al. 1989; Shim et al. 2000b; Sun et al. 2022; Yagi et al. 1989), and pure CaTiO₃ (Guennou et al. 2010). Opening squares of 17TiPv are decompression data. The dash lines are extrapolated regions without experimental data coverage. The unit-cell volumes were converted into molar volume to have the same standard. (Color online.)

adopts a tetragonal structure or orthorhombic structure, when Ti concentration is below and above CaTiO₃ 50%, respectively (Leinenweber et al. 1997; Sinelnikov et al. 1998). At ambient conditions, the radius of octahedral site Ti⁴⁺ is ~0.63 Å, and the radius of Si⁴⁺ is ~0.4 Å, with the former more compressible. From CaSiO₃ to Ca(Si_{0.5}Ti_{0.5})O₃, the crystal lattice has a more symmetric tetragonal structure dominated by Si⁴⁺. The crystal lattice may prefer its higher symmetry and smaller octahedral sites as more large-radius Ti atoms are introduced. As a result, K_0 may be more sensitive to the introduction of Ti atoms in this composition range. While from Ca(Si_{0.5}Ti_{0.5})O₃ to CaTiO₃, the crystal lattice is an orthorhombic structure and the SiO₈ or TiO₈ octahedral are already highly tilted, given that the octahedral sites are dominated by larger Ti⁴⁺. Since Ti⁴⁺ already dominates the lattice, elastic properties are largely controlled by Ti⁴⁺ that already exists; replacing more Si⁴⁺ with Ti⁴⁺ does not make K_0 decreases substantially with the Ti content from Ca(Si_{0.5}Ti_{0.5})O₃ to CaTiO₃.

Between pure CaSiO₃ davemaoite and 17TiPv, previous literature shows a confusing result, as K_0 of pure CaSiO₃ davemaoite reported by former studies is still controversial. If the K_0 is around 220–230 GPa as Chen et al. (2018); Shim et al. (2000b, 2000a), or Sun et al. (2022), had reported, the softening of K_0 is modest from the composition range of CaSiO₃ (~225 GPa) to 17TiPv (~209 GPa). Whereas, if the K_0 is around 250 GPa (Shim et al. 2002; Sun et al. 2016), there may be another linear relationship where K_0 drops less drastically than the range of 17TiPv to 25TiPv, but still a considerable drop. If the K_0 is around 280 GPa

TABLE 1. Equation of state parameters of Ca(Si,Ti)O₃ perovskite

Reference	Pressure medium	V_0 (cm ³) ^a	K_0 (GPa)	K'	Symmetry ^b	P_{max} (GPa) ^c
Ca(Si_{0.83}Ti_{0.17})O₃ Experiment						
This work	Ne	28.75(6)	224(2)	4(fixed)	Tet (<i>I4/mcm</i>)	82.4
Ca(Si_{0.75}Ti_{0.25})O₃ Experiment						
This work	Ne	29.68(5)	205(4)	4(fixed)	Tet (<i>P4/mmm</i>)	63.6
Ca(Si_{0.51}Ti_{0.49})O₃ Experiment						
Sinelnikov et al. (1998) ^d	N/A ^e	30.37(2)	185(5)	4(1)	Tet	15
Ca(Si_{0.23}Ti_{0.77})O₃ Experiment						
Sinelnikov et al. (1998) ^d	N/A ^e	32.48(2)	182(2)	4(1)	Orth	15
CaSiO₃ Experiment						
Mao et al. (1989)	N/A ^f	27.32(5)	281(4)	4	Cub	134
Yagi et al. (1989)	N/A ^f	27.45(4)	288(13)	4.0(2)	Cub	112
Tarrida and Richet (1989)	N/A ^f	27.46(6)	275(15)	4	Cub	96
Wang et al. (1996) ^d	N/A ^e	27.45(2)	232(8)	4.8(3)	Cub	12
Shim et al. (2000a) ^d	NaCl and Ar	27.45(1)	236(4)	3.9(2)	Cub	96
Shim et al. (2000b)	NaCl and Ar	27.45(3)	236(4)	3.9(2)	Cub	108
Shim et al. (2002)	Ar	27.45	255(5)	4	Tet	46
Ono et al. (2004) ^d	N/A ^f	27.63(2)	235(9)	4	Tet	106
Sun et al. (2016) ^d	NaCl	27.340(6)	249(4)	4	Tet	151
Chen et al. (2018)	Ne	27.820(6)	228(6)	4	Tet	62
Thomson et al. (2019) ^d	NaCl	27.76(4)	224(4)	4	Tet	13
Sun et al. (2022)	NaCl	27.46(2)	227(21)	4.0(3)	Tet	200
CaSiO₃ Computation						
Chizmeshya et al. (1996)	N/A	27.47	227	4.29	Cub	N/A
Jung and Oganov (2005)	N/A	28.24	219	4.08	Tet	N/A
Caracas et al. (2005)	N/A	26.82	249	4.09	Tet	N/A
Kawai and Tsuchiya (2014)	N/A	27.81	203.5	4.76	Cub	N/A
CaTiO₃ Experiment						
Fischer et al. (1993)	n-pentane and methyl-butane	33.87	177(3)	5.1(8)	Orth	3
Kung and Rigden (1999)	n-pentane and iso-pentane	34.17 (2)	175	5.78	Orth	3
Guennou et al. (2010)	N/A ^f	33.62 (7)	181.0(6)	4	Orth	60
Truffet et al. (2023) ^d	Ne	33.62 (7)	180.6(4)	4	Orth	170

Notes: The numbers in parentheses are uncertainties for the last digit. V_0 , K_0 , and K' without parentheses are assumed to be a fixed value.

^a Volume of per mole of chemical formula (calculated from unit-cell volume if not reported).

^b The symmetry column: Cub, Tet, and Orth represent cubic, tetragonal, and orthorhombic perovskite structures, respectively.

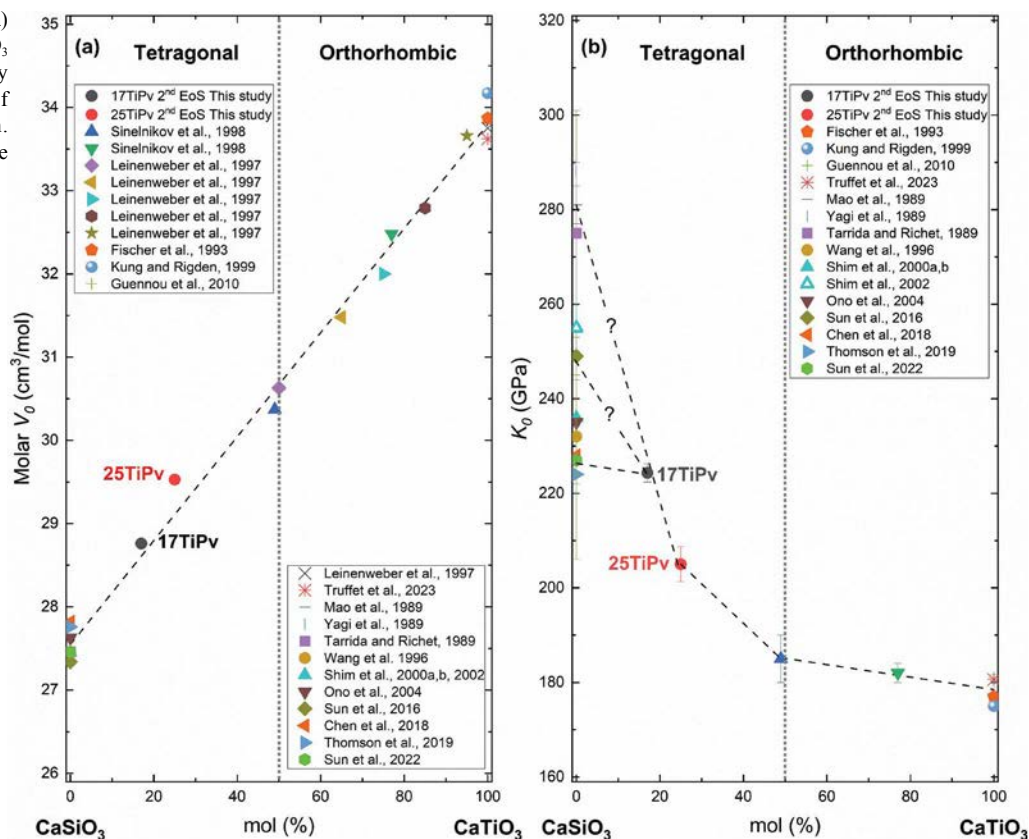
^c Maximum pressure with experimental data coverage.

^d Works of thermal equation of state; data coverage at 300 K might not be dense.

^e Multi-anvil press experiment and thus, pressure medium is not comparable to diamond-anvil cell experiments.

^f Did not load pressure medium or the pressure medium was not clearly mentioned by the literature.

FIGURE 5. Molar V_0 (a) and K_0 (b) of $\text{Ca}(\text{Si},\text{Ti})\text{O}_3$ solid solution reported by literature as function of CaTiO_3 molar fraction. The dash lines are to guide the eye. (Color online.)



(Mao et al. 1989; Tarrida and Richet 1989; Yagi et al. 1989), the K_0 decreases dramatically and linearly from CaSiO_3 to 25TiPv. A more complicated and nonlinear relationship between K_0 and Ti content across the entire composition range cannot be ruled out, due to the little consensus of elastic properties of pure CaSiO_3 davemaoite and among the literature.

Densities and elastic properties of $\text{Ca}(\text{Si},\text{Ti})\text{O}_3$ solid solutions

We calculated the density of 17TiPv and 25TiPv as a function of pressure based on their EoS's and chemical composition then compared their densities with the density of pure CaSiO_3 davemaoite (Shim et al. 2000b; Sun et al. 2022) and pure CaTiO_3 perovskite (Guennou et al. 2010) calculated from the EoS's in the literature (Fig. 6a). In Figure 6a, we plot the density of davemaoite calculated from Shim et al. (2000b) and Sun et al. (2022), because both studies were based on room temperature experiment, and their maximum pressure range is above 100 GPa summarized in Table 1. They have the same temperature conditions as this study and their data intensively cover most of the pressure range of the mantle. The EoS of davemaoite reported prior to 2000s with a higher K_0 (~270–280 GPa), i.e., Mao et al. (1989), Tarrida and Richet (1989), and Yagi et al. (1989), when the structure was constrained to a cubic configuration and the experiments were performed under relatively non-hydrastatic conditions (Table 1). Studies after the 2000s generally reported K_0 between 224 and 236 GPa and molar V_0 around 27.5 cm³, e.g., Ono et al. (2004), Shim et al. (2000a, 2000b), Sun et al. (2022), etc., leading to similar results as Shim

et al. (2000b) and Sun et al. (2022) in Figure 6a. For the density of CaTiO_3 perovskite, we plot the density calculated from Guennou et al. (2010). Although Truffet et al. (2023) has a greater pressure range, Truffet et al. (2023) is a thermal EoS study, and the data coverage at room temperature is sparse.

The density of $\text{Ca}(\text{Si},\text{Ti})\text{O}_3$ solid solutions under ambient conditions decreases monotonically with increasing Ti concentration (Fig. 6a). Adding Ti into the $\text{Ca}(\text{Si},\text{Ti})\text{O}_3$ solid solutions increases the formula weight of $\text{Ca}(\text{Si},\text{Ti})\text{O}_3$ solid solution. However, the unit-cell volume increases with increasing Ti content. As a result, the effect of the Ti-driving expansion of cell volume overwhelms the effect of formula weight increasing, and the net effect is the density decreasing. In addition, the K_0 decreases with rising Ti-contents, and thus, the unit-cell volume of $\text{Ca}(\text{Si},\text{Ti})\text{O}_3$ solid solutions shrinks more rapidly with rising Ti-content. As a result, the density of 25TiPv becomes similar to the density of 17TiPv at ~100 GPa. Nevertheless, the densities of 17TiPv and 25TiPv never reach the density of pure CaSiO_3 davemaoite even below 140 GPa. However, if the Ti content continues to increase, the crystal lattice becomes more compressible and the density rises more rapidly (see the rapid rise in the density increase of CaTiO_3 in Fig. 6). The CaTiO_3 is relatively more compressible, and its density exceeds the density of 25TiPv, 17TiPv, and CaSiO_3 at 25, 45, and 110 GPa, respectively.

GEOPHYSICAL IMPLICATIONS

We have determined the crystal structure, EoS, and densities of $\text{Ca}(\text{Si},\text{Ti})\text{O}_3$ perovskites with 17% and 25% Ti. The densities

of $\text{Ca}(\text{Si},\text{Ti})\text{O}_3$ perovskites were compared with those of the Preliminary Reference Earth Model (PREM) (Dziewonski and Anderson 1981), other major mantle minerals, e.g., ferropericlase, ringwoodite, and bridgmanite (Tange et al. 2009, 2012; Chang et al. 2015; Wolf et al. 2015), and pure tetragonal-structured CaSiO_3 perovskite (Shim et al. 2000b; Sun et al. 2022) in Figure 6a. Pure MgSiO_3 bridgmanite has a similar density as PREM; however, Fe-bearing $(\text{Mg}_{0.87}\text{Fe}_{0.13})\text{SiO}_3$ bridgmanite is a chemically more relevant phase for the mantle. Tschauner et al. (2021) reported that davemaioite adopts a cubic structure in the diamond inclusion, in contrary to most recent high-pressure results of tetragonal-structured CaSiO_3 as reported in Table 1. We therefore only compare our results with those for tetragonal-structured CaSiO_3 .

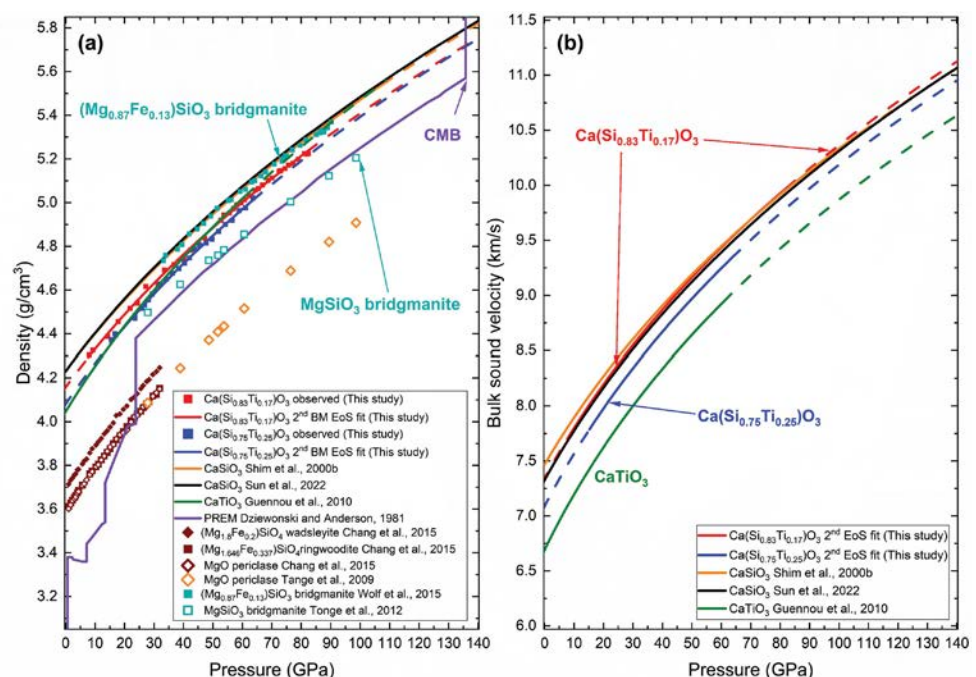
We first compare the 17TiPv and 25TiPv with CaSiO_3 perovskite and we found that 17TiPv and 25TiPv are less dense than pure tetragonal- CaSiO_3 perovskites in the investigated pressure ranges at 300 K. At the transition zone pressure of ~ 15 – 25 GPa, both 17TiPv and 25TiPv are ~ 0.05 – 0.1 g/cm^3 (or ~ 1 – 2%) less dense than pure tetragonal CaSiO_3 davemaioite (Sun et al. 2022), and $(\text{Mg}_{0.87}\text{Fe}_{0.13})\text{SiO}_3$ bridgmanite (Wolf et al. 2015). Although this study was conducted at 300 K, a pure CaSiO_3 davemaioite turns into cubic phase transition at the temperature as low as 490–580 K (Komabayashi et al. 2007), much lower than the temperature of cold slab. The 17TiPv and 25TiPv may also undergo such a phase transition. The tetragonal-cubic phase transition is a second-order phase transition without any volume change (Komabayashi et al. 2007). Consequently, the relative density difference between CaSiO_3 and that of 17TiPv and 25TiPv would still be $\sim 1\%$. By replacing the CaSiO_3 in the traditional model of MORB with Ti-bearing davemaioite, it is expected that the average density of MORB adapting Ti-bearing davemaioite is lower than that of conventional aspect.

Seismological studies have suggested that some subducting slabs become stagnant before penetrating deeper into the lower

mantle (Okino et al. 1989; Fukao et al. 1992, 2009; Fukao and Obayashi 2013). Several models have been proposed to explain the slab stagnation. (1) The negative Clapeyron slope of the ringwoodite to bridgmanite and ferro periclase transition (the post-spinel transition) and/or the delay of the onset of this transition due to the lower temperature of the slabs (Christensen and Yuen 1985; King et al. 2015). (2) Based on the first hypothesis, some studies suggested that the water in slabs makes the Clapeyron slope of the post-spinel transition negatively greater, and hence, water further favors slab stagnation (Litasov et al. 2005, 2006). (3) The slabs could also stagnate when it encounters a sudden increase in viscosity of the lower mantle (Gurnis and Hager 1988). (4) Some studies consider slab stagnation as a temporary geometry caused by trench retreat (Christensen 1996) or lateral mantle flow (Peng et al. 2021a, 2021b). Our results on densities of Ti-bearing CaSiO_3 perovskites may provide new insight into slab stagnation, as density changes due to phase transitions of mantle minerals play a key role in slab dynamics (Christensen and Yuen 1985; King et al. 2015; Litasov et al. 2006, 2005). 17TiPv and 25TiPv are ~ 1 – 2% less dense than pure CaSiO_3 (Fig. 6a). As the second most abundant phase in the subducted MORBs, the presence of Ti-bearing davemaioite may lower the density of the subducting slabs and thus can be among the factors contributing to their stagnation in the deep mantle.

Pure CaSiO_3 davemaioite is traditionally considered an “invisible” phase, due to its similar density with $(\text{Mg}_{0.87}\text{Fe}_{0.13})\text{SiO}_3$ bridgmanite (Fig. 6a). However, our results indicate that Ti-bearing davemaioites have lower densities than those of $(\text{Mg}_{0.87}\text{Fe}_{0.13})\text{SiO}_3$ bridgmanite and pure CaSiO_3 davemaioite, making them seismologically distinguishable within the lower mantle. The accumulation of subducted oceanic crust enriched with Ti-bearing davemaioite in the lowermost mantle may be responsible for the LLSVPs. Thomson et al. (2019) proposed that the LLSVPs can be explained by CaSiO_3 davemaioite based on the lower shear wave

FIGURE 6. (a) Comparison of the densities of $\text{Ca}(\text{Si},\text{Ti})\text{O}_3$ perovskites with PREM, as well as other common mineral phases from the transition zone to the lower mantle (Tange et al. 2009, 2012; Chang et al. 2015; Wolf et al. 2015). (b) K_T of $\text{Ca}(\text{Si},\text{Ti})\text{O}_3$ perovskites as a function of pressure calculated from their EoS values. (Color online.)



velocity of $\text{Ca}(\text{Si}_{0.6}\text{Ti}_{0.4})\text{O}_3$ observed with ultrasonic experiments. Due to the unavailability of shear wave velocity data at lower mantle conditions, we calculated the bulk sound velocity ($\sqrt{K/\rho}$, where K and ρ are bulk modulus and density, respectively) of pure CaSiO_3 davemaoite (Shim et al. 2000b; Sun et al. 2022), pure CaTiO_3 perovskite (Guennou et al. 2010), 17TiPv and 25TiPv from their EoS's as a reference (Fig. 6b). 25TiPv presents a lower bulk sound velocity than that of pure CaSiO_3 ; however, the bulk sound velocity of 17TiPv is similar to that of pure CaSiO_3 in the investigated pressure range. If the shear moduli (G) also follow the trend as bulk sound velocity in Figure 6b, the 17TiPv would have a similar G as CaSiO_3 , supporting Thomson's hypothesis with stoichiometrically more reasonable Ti content. 25TiPv with higher Ti content would have a lower G and thus would be more favorable for the formation of LLSVPs. Although the specific Ti concentration in the LLSVPs is unknown, the accumulation of oceanic crust with Ti-bearing davemaoites during the history of plate tectonics might increase the Ti content of davemaoite phase in the lower mantle stoichiometrically close to 25TiPv, in turn account for the LLSVPs in the lowermost mantle. However, the bulk sound velocity is a simplified reference to generally understand the seismic wave velocity of material. The definition of bulk sound velocity, $\sqrt{K/\rho}$, is not identical to either P wave velocity defined as

$$V_p = \sqrt{\left(K + \frac{3}{4}G\right) / \rho},$$

or S wave velocity defined as

$$V_s = \sqrt{G / \rho},$$

where shear modulus is indispensable to the calculation. Further investigations of the shear velocities and shear moduli of Ti-bearing davemaoite under lowermost mantle conditions are needed to support this hypothesis.

ACKNOWLEDGMENTS AND FUNDING

This work was supported by NSF grants EAR-2127807, EAR-1829273 to B.C. and in part supported by the Bullard award from the University of Hawaii at Mānoa to K.C. This work was carried out at GeoSoilEnviroCARS (The University of Chicago, Sector 13), Advanced Photon Source, Argonne National Laboratory. GeoSoilEnviroCARS is supported by the National Science Foundation-Earth Sciences (EAR-1128799) and Department of Energy-GeoSciences (DE-FG02-94ER14466). The use of gas loading system was supported by GeoSoilEnviroCARS and by the Consortium for Materials Properties Research in Earth Sciences (COMPRES) under National Science Foundation Cooperative Agreement EAR-1606856. This research used resources of the Advanced Photon Source, a U.S. Department of Energy (DOE) Office of Science User Facility operated for the DOE Office of Science by Argonne National Laboratory under Contract No. DE-AC02-06CH11357. We thank S. Tkachev and R. Rapp for technical support.

REFERENCES CITED

- Akber-Knutson, S., Bukowski, M.S.T., and Matas, J. (2002) On the structure and compressibility of CaSiO_3 perovskite. *Geophysical Research Letters*, 29, 4-1-4-4.
- Anzolini, C., Angel, R.J., Merlini, M., Derzi, M., Tokár, K., Milani, S., Krebs, M.Y., Brenker, F.E., Nestola, F., and Harris, J.W. (2016) Depth of formation of CaSiO_3 -walsstromite included in super-deep diamonds. *Lithos*, 265, 138-147, <https://doi.org/10.1016/j.lithos.2016.09.025>.
- Anzolini, C., Prencipe, M., Alvaro, M., Romano, C., Vona, A., Lorenzon, S., Smith, E.M., Brenker, F.E., and Nestola, F. (2018) Depth of formation of super-deep diamonds: Raman barometry of CaSiO_3 -walsstromite inclusions. *American Mineralogist. Journal of Earth and Planetary Materials*, 103, 69-74.
- Caracas, R., Wentzcovitch, R., Price, G.D., and Brodholt, J. (2005) CaSiO_3 perovskite at lower mantle pressures. *Geophysical Research Letters*, 32, L06306, <https://doi.org/10.1029/2004GL022144>.
- Chang, Y., Jacobsen, S.D., Bina, C.R., Thomas, S., Smyth, J.R., Frost, D.J., Boffa Ballaran, T., McCammon, C.A., Hauri, E.H., Inoue, T., and others (2015) Comparative compressibility of hydrous wadsleyite and ringwoodite: Effect of H_2O and implications for detecting water in the transition zone. *Journal of Geophysical Research: Solid Earth*, 120, 8259-8280.
- Chen, H., Shim, S.-H., Leinenweber, K., Prakapenka, V., Meng, Y., and Prescher, C. (2018) Crystal structure of CaSiO_3 perovskite at 28-62 GPa and 300 K under quasi-hydrostatic stress conditions. *American Mineralogist*, 103, 462-468, <https://doi.org/10.2138/am-2018-6087>.
- Chizmeshya, A.V.G., Wolf, G.H., and McMillan, P.F. (1996) First-principles calculation of the equation-of-state, stability, and polar optic modes of CaSiO_3 perovskite. *Geophysical Research Letters*, 23, 2725-2728, <https://doi.org/10.1029/96GL02624>.
- Christensen, U.R. (1996) The influence of trench migration on slab penetration into the lower mantle. *Earth and Planetary Science Letters*, 140, 27-39, [https://doi.org/10.1016/0012-821X\(96\)00023-4](https://doi.org/10.1016/0012-821X(96)00023-4).
- Christensen, U.R. and Yuen, D.A. (1985) Layered convection induced by phase transitions. *Journal of Geophysical Research*, 90, 10291-10300, <https://doi.org/10.1029/JB090iB12p10291>.
- Corgne, A. and Wood, B.J. (2005) Trace element partitioning and substitution mechanisms in calcium perovskites. *Contributions to Mineralogy and Petrology*, 149, 85-97, <https://doi.org/10.1007/s00410-004-0638-3>.
- Deschamps, F., Cobden, L., and Tackley, P.J. (2012) The primitive nature of large low shear-wave velocity provinces. *Earth and Planetary Science Letters*, 349-350, 198-208, <https://doi.org/10.1016/j.epsl.2012.07.012>.
- Dziewonski, A.M. and Anderson, D.L. (1981) Preliminary reference Earth model. *Physics of the Earth and Planetary Interiors*, 25, 297-356, [https://doi.org/10.1016/0031-9201\(81\)90046-7](https://doi.org/10.1016/0031-9201(81)90046-7).
- Fei, Y., Ricolleau, A., Frank, M., Mibe, K., Shen, G., and Prakapenka, V. (2007) Toward an internally consistent pressure scale. *Proceedings of the National Academy of Sciences of the United States of America*, 104, 9182-9186, <https://doi.org/10.1073/pnas.0609013104>.
- Fischer, G.J., Wang, Z., and Karato, S. (1993) Elasticity of CaTiO_3 , SrTiO_3 and BaTiO_3 perovskites up to 3.0 GPa: The effect of crystallographic structure. *Physics and Chemistry of Minerals*, 20, 97-103, <https://doi.org/10.1007/BF00207202>.
- Frost, D.A. and Rost, S. (2014) The P-wave boundary of the Large-Low Shear Velocity Province beneath the Pacific. *Earth and Planetary Science Letters*, 403, 380-392, <https://doi.org/10.1016/j.epsl.2014.06.046>.
- Fukao, Y. and Obayashi, M. (2013) Subducted slabs stagnant above, penetrating through, and trapped below the 660 km discontinuity. *Journal of Geophysical Research: Solid Earth*, 118, 5920-5938, <https://doi.org/10.1002/2013JB010466>.
- Fukao, Y., Obayashi, M., Inoue, H., and Nenbai, M. (1992) Subducting slabs stagnant in the mantle transition zone. *Journal of Geophysical Research*, 97, 4809-4822, <https://doi.org/10.1029/91JB02749>.
- Fukao, Y., Widiyantoro, S., and Obayashi, M. (2001) Stagnant slabs in the upper and lower mantle transition region. *Reviews of Geophysics*, 39, 291-323, <https://doi.org/10.1029/1999RG000068>.
- Fukao, Y., Obayashi, M., Nakakuki, T., and the Deep Slab Project Group. (2009) Stagnant slab: A review. *Annual Review of Earth and Planetary Sciences*, 37, 19-46, <https://doi.org/10.1146/annurev.earth.36.031207.124224>.
- Gale, A., Dalton, C.A., Langmuir, C.H., Su, Y., and Schilling, J.-G. (2013) The mean composition of ocean ridge basalts. *Geochemistry, Geophysics, Geosystems*, 14, 489-518, <https://doi.org/10.1029/2012GC004334>.
- Gonzalez-Platas, J., Alvaro, M., Nestola, F., and Angel, R. (2016) EosFit7-GUI: A new graphical user interface for equation of state calculations, analyses and teaching. *Journal of Applied Crystallography*, 49, 1377-1382, <https://doi.org/10.1107/S1600576716008050>.
- Guennou, M., Bouvier, P., Krikler, B., Kreisel, J., Haumont, R., and Garbarino, G. (2010) High-pressure investigations of CaTiO_3 up to 60 GPa using X-ray diffraction and Raman spectroscopy. *Physical Review B*, 82, 134101, <https://doi.org/10.1103/PhysRevB.82.134101>.
- Gurnis, M. and Hager, B.H. (1988) Controls of the structure of subducted slabs. *Nature*, 335, 317-321, <https://doi.org/10.1038/335317a0>.
- Hernlund, J.W. and Houser, C. (2008) On the statistical distribution of seismic velocities in Earth's deep mantle. *Earth and Planetary Science Letters*, 265, 423-437, <https://doi.org/10.1016/j.epsl.2007.10.042>.
- Hirose, K., Shimizu, N., van Westrenen, W., and Fei, Y. (2004) Trace element partitioning in Earth's lower mantle and implications for geochemical consequences of partial melting at the core-mantle boundary. *Physics of the Earth and Planetary Interiors*, 146, 249-260, <https://doi.org/10.1016/j.pepi.2002.11.001>.
- Hirose, K., Takafuji, N., Sata, N., and Ohishi, Y. (2005) Phase transition and density of subducted MORB crust in the lower mantle. *Earth and Planetary Science Letters*, 237, 239-251, <https://doi.org/10.1016/j.epsl.2005.06.035>.
- Jung, D.Y. and Oganov, A.R. (2005) Ab initio study of the high-pressure behavior of CaSiO_3 perovskite. *Physics and Chemistry of Minerals*, 32, 146-153, <https://doi.org/10.1007/s00269-005-0453-z>.
- Kaminsky, F. (2012) Mineralogy of the lower mantle: A review of 'super-deep' mineral inclusions in diamond. *Earth-Science Reviews*, 110, 127-147, <https://doi.org/10.1016/j.earscirev.2011.10.005>.
- Kawai, K. and Tsuchiya, T. (2014) P - V - T equation of state of cubic CaSiO_3 perovskite

- from first-principles computation. *Journal of Geophysical Research: Solid Earth*, 119, 2801–2809, <https://doi.org/10.1002/2013JB010905>.
- Kesson, S.E., Fitz Gerald, J.D., and Shelley, J.M.G. (1994) Mineral chemistry and density of subducted basaltic crust at lower-mantle pressures. *Nature*, 372, 767–769, <https://doi.org/10.1038/372767a0>.
- Kesson, S.E., Fitz Gerald, J.D., and Shelley, J.M. (1998) Mineralogy and dynamics of a pyrolytic lower mantle. *Nature*, 393, 252–255, <https://doi.org/10.1038/30466>.
- King, S.D., Frost, D.J., and Rubie, D.C. (2015) Why cold slabs stagnate in the transition zone. *Geology*, 43, 231–234, <https://doi.org/10.1130/G36320.1>.
- Komabayashi, T., Hirose, K., Sata, N., Ohishi, Y., and Dubrovinsky, L.S. (2007) Phase transition in CaSiO₃ perovskite. *Earth and Planetary Science Letters*, 260, 564–569, <https://doi.org/10.1016/j.epsl.2007.06.015>.
- Kudo, Y., Hirose, K., Murakami, M., Asahara, Y., Ozawa, H., Ohishi, Y., and Hirao, N. (2012) Sound velocity measurements of CaSiO₃ perovskite to 133 GPa and implications for lowermost mantle seismic anomalies. *Earth and Planetary Science Letters*, 349–350, 1–7, <https://doi.org/10.1016/j.epsl.2012.06.040>.
- Kung, J. and Rigden, S. (1999) Oxide perovskites: Pressure derivatives of the bulk and shear moduli. *Physics and Chemistry of Minerals*, 26, 234–241, <https://doi.org/10.1007/s002690050182>.
- Leinenweber, K., Grzechnik, A., Voorhees, M., Navrotsky, A., Yao, N., and McMillan, P.F. (1997) Structural variation in Ca(Ti,Si_{1-x})O₃ perovskites (1 < x < 0.65) and the ordered phase Ca₂TiSiO₆. *Physics and Chemistry of Minerals*, 24, 528–534, <https://doi.org/10.1007/s002690050068>.
- Litasov, K., Ohtani, E., Sano, A., Suzuki, A., and Funakoshi, K. (2005) Wet subduction versus cold subduction. *Geophysical Research Letters*, 32, L13312, <https://doi.org/10.1029/2005GL022921>.
- Litasov, K., Ohtani, E., and Sano, A. (2006) Influence of water on major phase transitions in the Earth's Mantle. In S.D. Jacobsen and S. Van Der Lee, Eds., *Geophysical Monograph Series*, 95–111. American Geophysical Union.
- Liu, L.-G. and Ringwood, A.E. (1975) Synthesis of a perovskite-type polymorph of CaSiO₃. *Earth and Planetary Science Letters*, 28, 209–211, [https://doi.org/10.1016/0012-821X\(75\)90229-0](https://doi.org/10.1016/0012-821X(75)90229-0).
- Mao, H.K., Chen, L.C., Hemley, R.J., Jephcoat, A.P., Wu, Y., and Bassett, W.A. (1989) Stability and equation of state of CaSiO₃-perovskite to 134 GPa. *Journal of Geophysical Research*, 94 (B12), 17889–17894, <https://doi.org/10.1029/JB094iB12p17889>.
- Milani, S., Comboni, D., Lotti, P., Fumagalli, P., Zibera, L., Maurice, J., Hanfland, M., and Merlini, M. (2021) Crystal structure evolution of CaSiO₃ polymorphs at Earth's mantle pressures. *Minerals*, 11, 652, <https://doi.org/10.3390/min11060652>.
- Murakami, M., Hirose, K., Sata, N., and Ohishi, Y. (2005) Post-perovskite phase transition and mineral chemistry in the pyrolytic lowermost mantle. *Geophysical Research Letters*, 32, L03304, <https://doi.org/10.1029/2004GL021956>.
- Nestola, F., Korolev, N., Kopylova, M., Rotiroli, N., Pearson, D.G., Pamato, M.G., Alvaro, M., Peruzzo, L., Gurney, J.J., Moore, A.E., and others. (2018) CaSiO₃ perovskite in diamond indicates the recycling of oceanic crust into the lower mantle. *Nature*, 555, 237–241, <https://doi.org/10.1038/nature25972>.
- Okino, K., Ando, M., Kaneshima, S., and Hirahara, K. (1989) The horizontally lying slab. *Geophysical Research Letters*, 16, 1059–1062, <https://doi.org/10.1029/GL016i009p1059>.
- Ono, S., Ohishi, Y., and Mibe, K. (2004) Phase transition of Ca-perovskite and stability of Al-bearing Mg-perovskite in the lower mantle. *American Mineralogist*, 89, 1480–1485, <https://doi.org/10.2138/am-2004-1016>.
- Peng, D., Liu, L., and Wang, Y. (2021a) A newly discovered late-Cretaceous East Asian Flat Slab explains its unique lithospheric structure and tectonics. *Journal of Geophysical Research: Solid Earth*, 126, e2021JB022103, <https://doi.org/10.1029/2021JB022103>.
- Peng, D., Liu, L., Hu, J., Li, S., and Liu, Y. (2021b) Formation of East Asian Stagnant Slabs due to a pressure-driven Cenozoic mantle wind following Mesozoic subduction. *Geophysical Research Letters*, 48, e2021GL094638, <https://doi.org/10.1029/2021GL094638>.
- Prescher, C. and Prakapenka, V.B. (2015) DIOPTAS: A program for reduction of two-dimensional X-ray diffraction data and data exploration. *High Pressure Research*, 35, 223–230, <https://doi.org/10.1080/08957959.2015.1059835>.
- Ricolleau, A., Perrillat, J.-P., Fiquet, G., Daniel, I., Matas, J., Addad, A., Menguy, N., Cardon, H., Mezouar, M., and Guignot, N. (2010) Phase relations and equation of state of a natural MORB: Implications for the density profile of subducted oceanic crust in the Earth's lower mantle. *Journal of Geophysical Research*, 115, B08202, <https://doi.org/10.1029/2009JB006709>.
- Ringwood, A.E. (1962) A model for the upper mantle. *Journal of Geophysical Research*, 67, 857–867, <https://doi.org/10.1029/JZ067i002p00857>.
- Rivers, M., Prakapenka, V., Kubo, A., Pullins, C., Holl, C., and Jacobsen, S. (2008) The COMPRES/GSECARS gas-loading system for diamond anvil cells at the Advanced Photon Source. *High Pressure Research*, 28, 273–292, <https://doi.org/10.1080/08957950802333593>.
- Seto, Y., Nishio-Hamane, D., Nagai, T., and Sata, N. (2010) Development of a software suite on X-ray diffraction experiments. *The Review of High Pressure Science and Technology*, 20, 269–276, <https://doi.org/10.4131/jshpreview.20.269>.
- Shim, S.-H. (2017) Pytheos-a python tool set for equations of state. Zenodo. <http://doi.org/10.5281/zenodo.802392>.
- (2020) PeakPo: More complete 7.7.30 with all major bugs fixed. Zenodo. <http://doi.org/10.5281/zenodo.3726423>.
- Shim, S.-H., Duffy, T.S., and Shen, G. (2000a) The equation of state of CaSiO₃ perovskite to 108 GPa at 300 K. *Physics of the Earth and Planetary Interiors*, 120, 327–338, [https://doi.org/10.1016/S0031-9201\(00\)00154-0](https://doi.org/10.1016/S0031-9201(00)00154-0).
- (2000b) The stability and P-V-T equation of state of CaSiO₃ perovskite in the Earth's lower mantle. *Journal of Geophysical Research*, 105, 25955–25968, <https://doi.org/10.1029/2000JB900183>.
- Shim, S.-H., Jeanloz, R., and Duffy, T.S. (2002) Tetragonal structure of CaSiO₃ perovskite above 20 GPa. *Geophysical Research Letters*, 29, 19–19–14.
- Sinelnikov, Y.D., Chen, G., and Liebermann, R.C. (1998) Elasticity of CaTiO₃-CaSiO₃ perovskites. *Physics and Chemistry of Minerals*, 25, 515–521, <https://doi.org/10.1007/s002690050143>.
- Steeve, G., Irifune, T., Higo, Y., and Tange, Y. (2019) Sound velocities of CaSiO₃ perovskite and its implications for the deep mantle mineralogy, 2019, MR24A-03. Presented at the AGU Fall Meeting Abstracts.
- Stixrude, L. and Lithgow-Bertelloni, C. (2012) Geophysics of chemical heterogeneity in the mantle. *Annual Review of Earth and Planetary Sciences*, 40, 569–595, <https://doi.org/10.1146/annurev.earth.36.031207.124244>.
- Sun, N., Mao, Z., Yan, S., Wu, X., Prakapenka, V.B., and Lin, J.-F. (2016) Confirming a pyrolytic lower mantle using self-consistent pressure scales and new constraints on CaSiO₃ perovskite. *Journal of Geophysical Research: Solid Earth*, 121, 4876–4894, <https://doi.org/10.1002/2016JB013062>.
- Sun, N., Bian, H., Zhang, Y., Lin, J.-F., Prakapenka, V.B., and Mao, Z. (2022) High-pressure experimental study of tetragonal CaSiO₃-perovskite to 200 GPa. *American Mineralogist*, 107, 110–115, <https://doi.org/10.2138/am-2021-7913>.
- Tamai, H. and Yagi, T. (1989) High-pressure and high-temperature phase relations in CaSiO₃ and CaMgSi₂O₆ and elasticity of perovskite-type CaSiO₃. *Physics of the Earth and Planetary Interiors*, 54, 370–377, [https://doi.org/10.1016/0031-9201\(89\)90254-9](https://doi.org/10.1016/0031-9201(89)90254-9).
- Tange, Y., Nishihara, Y., and Tsuchiya, T. (2009) Unified analyses for P-V-T equation of state of MgO: A solution for pressure-scale problems in high-P-T experiments. *Journal of Geophysical Research*, 114, B03208, <https://doi.org/10.1029/2008JB005813>.
- Tange, Y., Kuwayama, Y., Irifune, T., Funakoshi, K., and Ohishi, Y. (2012) P-V-T equation of state of MgSiO₃ perovskite based on the MgO pressure scale: A comprehensive reference for mineralogy of the lower mantle: P-V-T EOS of MgSiO₃ perovskite. *Journal of Geophysical Research: Solid Earth*, 117, B06201.
- Tarrida, M. and Richet, P. (1989) Equation of state of CaSiO₃ perovskite to 96 GPa. *Geophysical Research Letters*, 16, 1351–1354, <https://doi.org/10.1029/GL016i011p1351>.
- Thomson, A.R., Walter, M.J., Kohn, S.C., and Brooker, R.A. (2016) Slab melting as a barrier to deep carbon subduction. *Nature*, 529, 76–79, <https://doi.org/10.1038/nature16174>.
- Thomson, A.R., Crichton, W.A., Brodholt, J.P., Wood, I.G., Siersch, N.C., Muir, J.M.R., Dobson, D.P., and Hunt, S.A. (2019) Seismic velocities of CaSiO₃ perovskite can explain LLSVPs in Earth's lower mantle. *Nature*, 572, 643–647, <https://doi.org/10.1038/s41586-019-1483-x>.
- Truffet, B., Fiquet, G., Morard, G., Baron, M.A., Miozzi, F., Harmand, M., Ravasio, A., Mezouar, M., and Guyot, F. (2023) High pressure dissociation of CaTiO₃ perovskite into CaO and CaTi₂O₇. *Physics of the Earth and Planetary Interiors*, 334, 106968, <https://doi.org/10.1016/j.pepi.2022.106968>.
- Tschauner, O., Huang, S., Yang, S., Humayun, M., Liu, W., Gilbert Corder, S.N., Bechtel, H.A., Tischler, J., and Rossman, G.R. (2021) Discovery of davemaoite, CaSiO₃-perovskite, as a mineral from the lower mantle. *Science*, 374, 891–894, <https://doi.org/10.1126/science.abb8568>.
- Wang, Y., Weidner, D.J., and Guyot, F. (1996) Thermal equation of state of CaSiO₃ perovskite. *Journal of Geophysical Research*, 101, 661–672, <https://doi.org/10.1029/95JB03254>.
- Wolf, A.S., Jackson, J.M., Dera, P., and Prakapenka, V.B. (2015) The thermal equation of state of (Mg,Fe)SiO₃ bridgmanite (perovskite) and implications for lower mantle structures. *Journal of Geophysical Research: Solid Earth*, 120, 7460–7489, <https://doi.org/10.1002/2015JB012108>.
- Yagi, T., Kusanagi, S., Tsuchida, Y., and Fukai, Y. (1989) Isothermal compression and stability of perovskite-type CaSiO₃. *Proceedings of the Japan Academy. Series B, Physical and Biological Sciences*, 65, 129–132, <https://doi.org/10.2183/pjab.65.129>.

MANUSCRIPT RECEIVED JUNE 16, 2023

MANUSCRIPT ACCEPTED FEBRUARY 14, 2024

ACCEPTED MANUSCRIPT ONLINE FEBRUARY 28, 2024

MANUSCRIPT HANDLED BY ZHICHENG JING

Endnote:

¹Deposit item AM-24-119104. Online Materials are free to all readers. Go online, via the table of contents or article view, and find the tab or link for supplemental materials. The CIF has been peer-reviewed by our Technical Editors.